Study on the Optical Properties, Crystal Growth and Photocatalytic Activity of Ni-doped TiO2 Nanoparticles

P. Guo, L. Guo

This document appeared in

Detlef Stolten, Thomas Grube (Eds.):
18th World Hydrogen Energy Conference 2010 - WHEC 2010
Parallel Sessions Book 3: Hydrogen Production Technologies - Part 2
Proceedings of the WHEC, May 16.-21. 2010, Essen
Schriften des Forschungszentrums Jülich / Energy & Environment, Vol. 78-3
Institute of Energy Research - Fuel Cells (IEF-3)
Forschungszentrum Jülich GmbH, Zentralbibliothek, Verlag, 2010
ISBN: 978-3-89336-653-8

Study on the Optical Properties, Crystal Growth and Photocatalytic Activity of Ni-doped TiO_2 Nanoparticles

Penghui Guo, State Key laboratory of Multiphase Flow in Power Engineering, Xi'an Jiaotong University, China
Liejin Guo,State Key laboratory of Multiphase Flow in Power Engineering, Xi'an Jiaotong University, China

TiO_2, as a widely used material for photocatalysis, is attracting more and more attention [1-5]. Up to date, a great deal of methods are under research to enhance its photocatalytic activity, for example, doping TiO_2 with metal ion or nonmetal ion [6, 7], loading TiO_2 with expensive metals [8, 9], sensitizing TiO_2 with dyes [10-12] or other methods [13, 14] etc. Ni is a low-price metal and of high activity in industrial catalysis, and it is also used in photocatalytic reactions to lengthen the absorption band of catalysts [15]. Nevertheless, systematic experimental studies regarding the influence of the doping ion to the main body TiO_2 are still lacking, especially the photoexcited carriers changing. In the present work, a series of porous and nano-structured Ni-doped TiO_2 with anatase structure are synthesized by ultrasonic sol-gel method. The structure, photophysical and photochemical properties are well discussed in this paper. What's more, the photoluminescence spectra were used to compare the photo charge carries transfer before and after Ni doping.

All chemicals used were of analytical grade without further purification. Firstly TBOT was dispersed in methanol with PEG-6000 and proper glacial acetic acid. Then the sol was dropped into acetic acid aqueous solution along with ultrasonic under room temperature. As for the Ni-TiO_2, the $Ni(NO_3)_2{\cdot}2H_2O$ were added into the aqueous solution to give doping level from 0%-10%. The mixture was evaporated in a water bath under 343K after 3h ultrasonic reaction. The gel was dried in vacuum at 343K for 8h. The product was finally heated in air at 723K for 4h.X-ray diffraction patterns of the samples were obtained from a PANalytical X'pert Pro diffractometer using Cu Kα irradiation. N_2 adsorption-desorption isotherms at 77K were measured using a Beckman Coulter SA 3100 instrument. Uv-vis adsorption spectra were determined by Hitachi U-4100 UV-vis-near IR spectrophotometer with $BaSO_4$ as the reference. Fluorescence emission and excitation spectra were got from PTI QM4 fluorescent photometer using a 75W Xe lamp as the exciting light resource and a filter is used to cut off the scattering light between the sample and detector.Photocatalytic hydrogen evolution was tested in a side-irradiation pyrex cell. A 350 W Xe lamp was used as the light source. Hydrogen evolved was analyzed by an on-line thermal conductivity detector (TCD) gas chromatograph (NaX zeolite column, nitrogen as a carrier gas). In all experiments, 200ml of 20 vol% aqueous methanol solution containing 0.1g catalyst was added into the cell.

N_2 adsorption-desorption results for Ni-TiO_2 with Ni doping of 5% and 0% are shown in Fig.1. Actually all the samples give typical H_1-type N_2 adsorption-desorption isotherms with obvious hysteresis loops proving the mesopores of large size. The small figuration shows that the pore sizes are smaller than 20nm compared with after Ni doping. The BET surface area of samples increased from 127 m^2/g to 148m^2/g when the amount of Ni doping increased from

0% to 5%, while the BET surface area for Ni doping of 10% is 144m^2/g. The total pore volume decreased from 0.51ml/g to 0.34 ml/g when the doping amount increased from 0% to 10%.

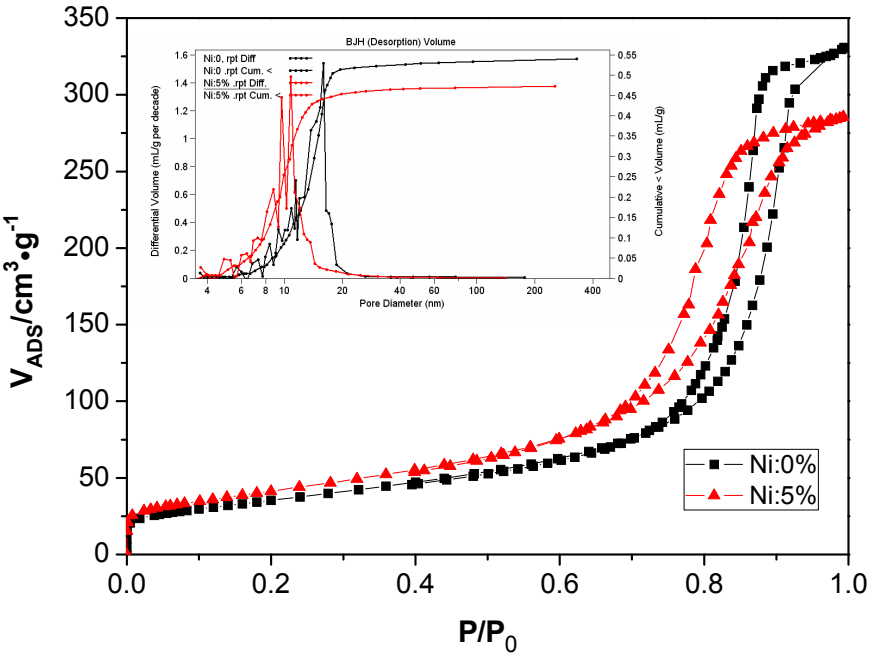

Figure 1: N_2 adsorption-desorption isotherms at 77K for Ni-TiO_2 with Ni^{2+} doping of 5% and 0% respectively.

TEM images for TiO_2 with Ni^{2+} doping of 0% and 5% are shown in Fig.2. The TiO_2 with or without Ni are both very homogenous particle distribution due to the dispersing role of ultrosonication. Considering the particle shape, both samples are anatase of cubic nanoparticles. It can also be seen that the particle size of Ni-TiO_2 is smaller than TiO_2 without Ni doping under high resolution transmission electron microscopy. Giving the result of the EDS, the grains we see from TEM are polycrystals. However, the TEM images also show that the product is not mesopore structure as the N_2 adsorption-desorption isotherms indicate. It is supposed that the crystals are growing uniformly because of ultrasonic process and piled up forming pores.

Fig.3 shows the XRD patterns of TiO_2 with various Ni doping calcined at 723K. It can be seen only the sample with 10% Ni doping is not pure anatase. The peak at 2θ=43.2°, which only can be seen when the doping amount increases to 10%, is identified as the characterized peak of cubic NiO (h=2, l=k=0). The mean size of the crystallites in samples can be estimated by the FWHM of the XRD peak at 2θ=25.3° using the Debye-Scherrer equation. Although the further crystallization of TiO_2 particles is a main process at a lower annealing temperature [16], the crystallite size decreases from 11nm to 9nm with increasing Ni doping from 0% to 5%, which may cause by the Ni-O bond distance (1.87 Å) shorter that the Ti-O bond distance(1.94 Å) [17]. On condition that, we can say that Ni has entered the framework of TiO_2 crystals. Combined with N_2 ads-des isotherms and XRD results, it can be concluded

that Ni doping can restrain the particle growth and inhibit the formation of rutile crystallites in the matrix of mesoprous TiO_2 at a higher calcination temperature before NiO appears. It also indicates that the ultrasonic method can have a larger doping amount than other methods [15].

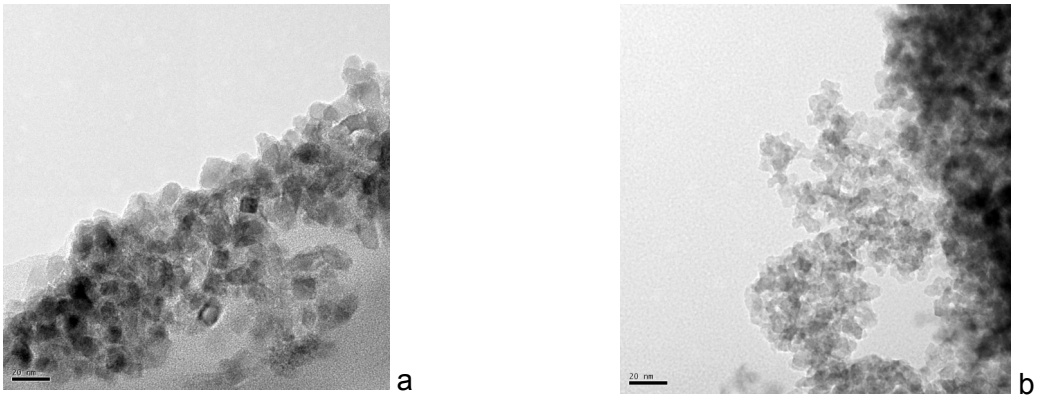

Figure 2: TEM images of TiO_2 with Ni^{2+} doping of 0% and 5%. (a: TiO_2; b: Ni-TiO_2).

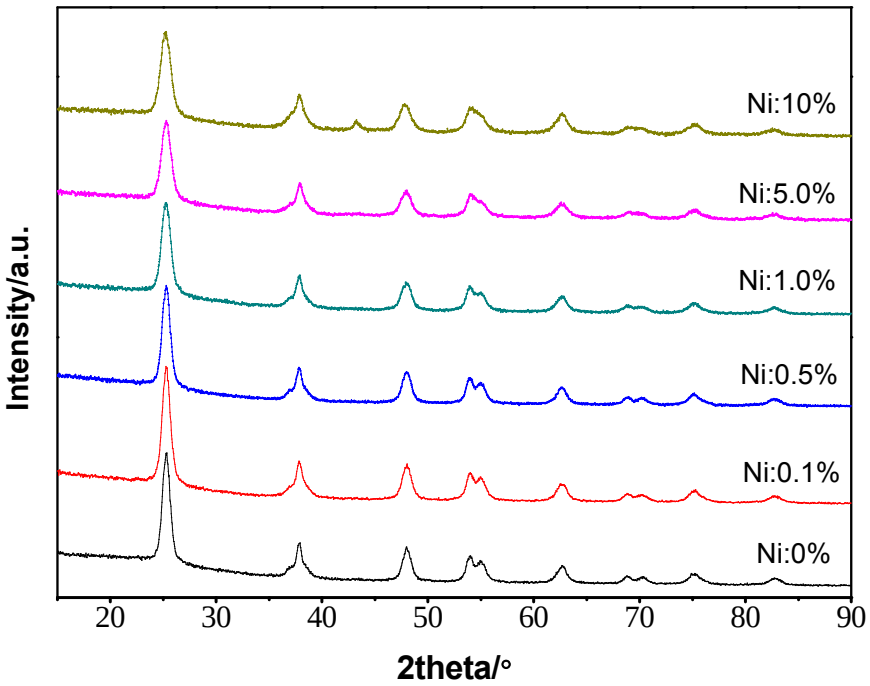

Figure 3: XRD diagram of various TiO_2 with increasing doping; all samples were calcined at 723K.

Raman scattering is a more sensitive detection technique of nanocrystal structure characterization. Five peaks showed in the spectra are attributed to the antase phase Raman scattering model of $A_{1g}+2B_{1g}+3E_g$. The Raman scattering did not detect the NiO of TiO_2 with a doping amount of 5%. We can say that by using this ultrasonication method a large

amount of Ni^{2+}, as a substitution for Ti^{4+}, were successfully synthesized, incorporating into the matrix of TiO_2. The bands of TiO_2 with Ni doping are 123cm^{-1}(E_g), 177cm^{-1}(E_g), 374cm^{-1}(B_{1g}), 497cm^{-1}(A_{1g}, B_{1g}), 621cm^{-1}(E_g), have a small red shift and broadening change distinguished from the TiO_2 without Ni doping, whose peaks are 125cm^{-1}(E_g), 179cm^{-1}(E_g), 376cm^{-1}(B_{1g}), 498cm^{-1}(A_{1g}, B_{1g}), 622cm^{-1}(E_g). Compared to the P25 (commercial TiO_2 with a surface area of 55 m^2/g), the Raman scattering bands of all the TiO_2 samples prepared by ultrasonication method have an obvious red shift and broadening. This shift and broadening are caused by photon relaxation due to the defects or oxygen vacancies of the nanocrystals, the same results as our former research[18].

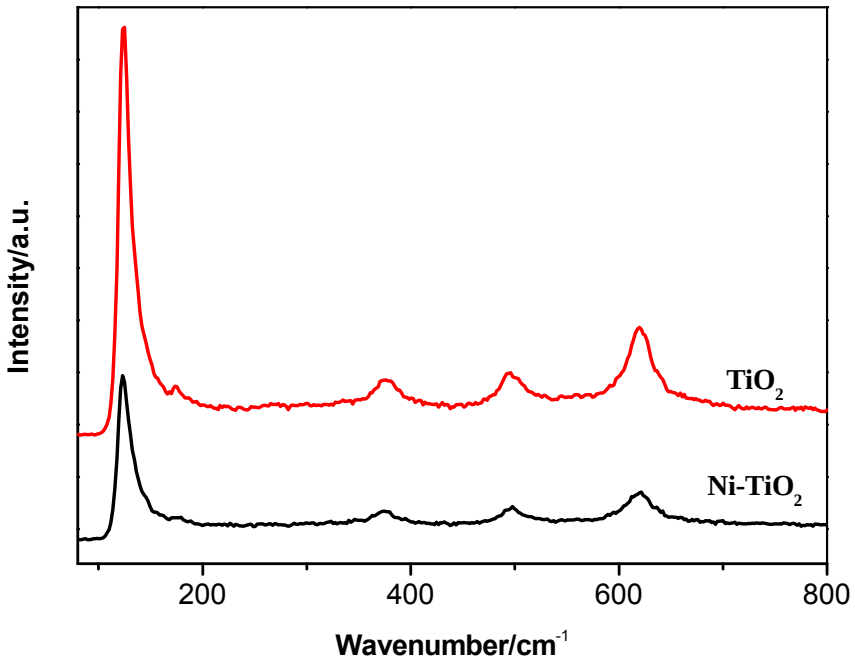

Figure 4: Raman of TiO_2 and TiO_2 with 5% Ni doping.

Fig.5 shows the UV-VIS-NIR absorbance of Ni-TiO_2. The bands at near infrared area for all the samples are due to bending and symmetric or asymmetric stretching vibration modes of the H_2O molecules adsorbed on the surface of the samples [19]. TiO_2 with Ni doping has a visible light response due to the formation of impurity energy level. The absorption band around 750nm is supposed to be due to the oxygen vacancies formation in virtue of the imbalance of charges caused by Ni doping. The band gap energy of the pure TiO_2 is 3.28eV calculated by K-M equations, a little bigger than reported, which may be caused by the quantum size effect as the particle size is around 10nm more or less with the Bore radius of TiO_2 [20].

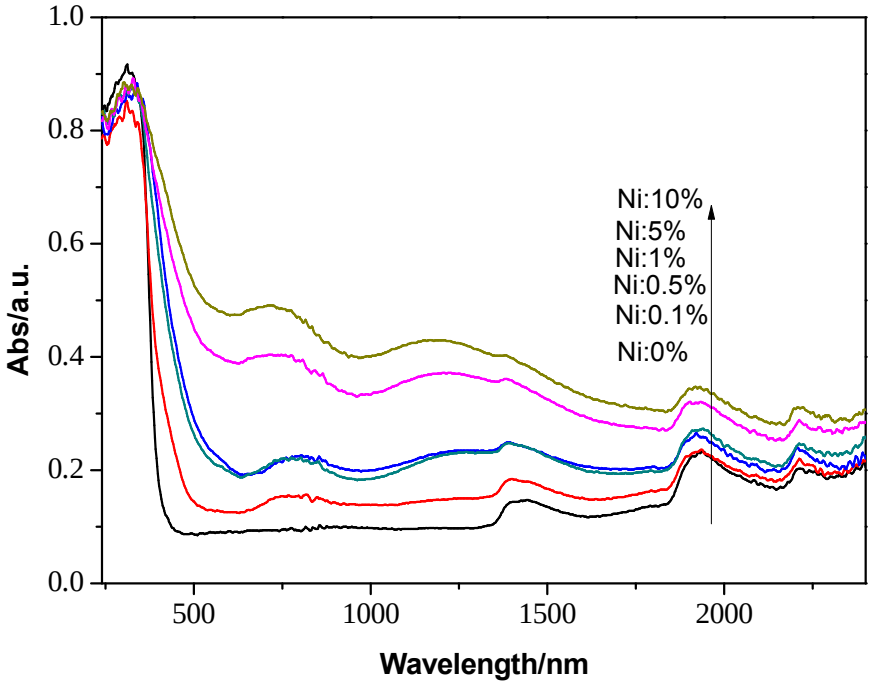

Figure 5: UV-VIS-NIR absorbance spectra of Ni doped TiO_2.

There are three Gaussian-type peaks at 358, 378, 394 showed in PL excitation spectrum. The 378nm peak is engendered by electron transition from valence band to conduction band on base of the band gap energy. The other two peaks may be caused by the vibration energy level in the CB and VB or free exciton absorption band around CB and VB [21]. Stokes shift is obviously observed because of indirect transition and the vibration energy level in energy band. Based on the symmetry property of excitation and emission, the 436nm emission band stems from conduction band to valence band direct recombination. The emission band observed in fig.6 (b) around 825nm is supposed to be caused by the intrinsic defects of anatase TiO_2 [22]. When Ni is doped in the frame of TiO_2, the quantum-size effect makes the emission band a little blue-shift, and this is in accordance with the crystal growth results.

It is very interesting that when TiO_2 has a very small doping amount of Ni, it hardly emits, which is probably resulted from that Ni^{2+} dispersed in the TiO_2 trapped the excited electron and relaxed them through a non-radiative way. But the amount is limited so the photocatalytic activity decreased a little. As the amount of Ni increasing, the impure energy levels generate, as we can see from the fig.6(d), it emits along with the conduction band of TiO_2 for the emission band is blueshifting. The optimal amount exists because the excessive Ni would become trapping center of photo excited holes. The hydrogen evolution amount has a same tendency with the PL emission spectra. It is supposed that Ni has two roles in doping TiO_2. One is when Ni is dispersed in TiO_2 bulk with very small amount, excited electrons are trapped by Ni and then relaxed non-rediatively, so the electrons can't migrate to the TiO_2 surface and reduce H^+. But this influence is not big enough for the Ni amount limited. The other role is the excited electrons are transiently trapped by the level and then released to transfer to TiO_2 surface when Ni has an abundant amount to generate new impure energy level in TiO_2. The Ni-doped TiO_2 has visible light absorption but no photocatalytic hydrogen

production activity under visible light. One reasonable possibility is that a deep energy level is yielded in TiO_2 with Ni doping. The location of the impure energy level will be discussed in next work.

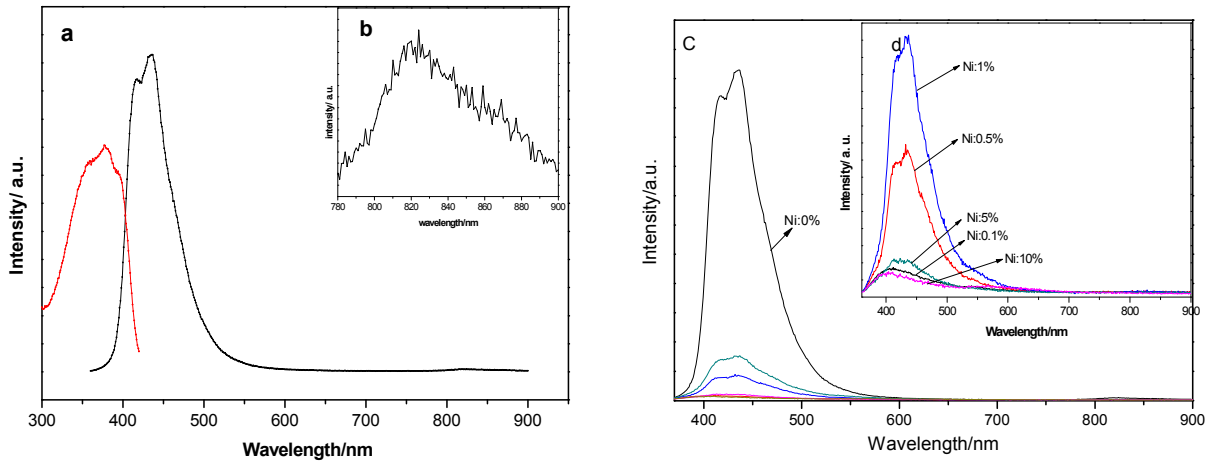

Figure 6: Fluorescence excitation and emission spectra of TiO_2 (all the PL emissions are excited by 340nm with a cut-off filterλ≥350nm and the PL excitations are collected with a band-pass filter at λ=441.6nm. a: nondoped TiO_2, b: the enlarged figuration from 700nm to 900nm; c: TiO_2 doped with different amount of Ni; d: the enlarged figuration of Ni doping TiO_2).

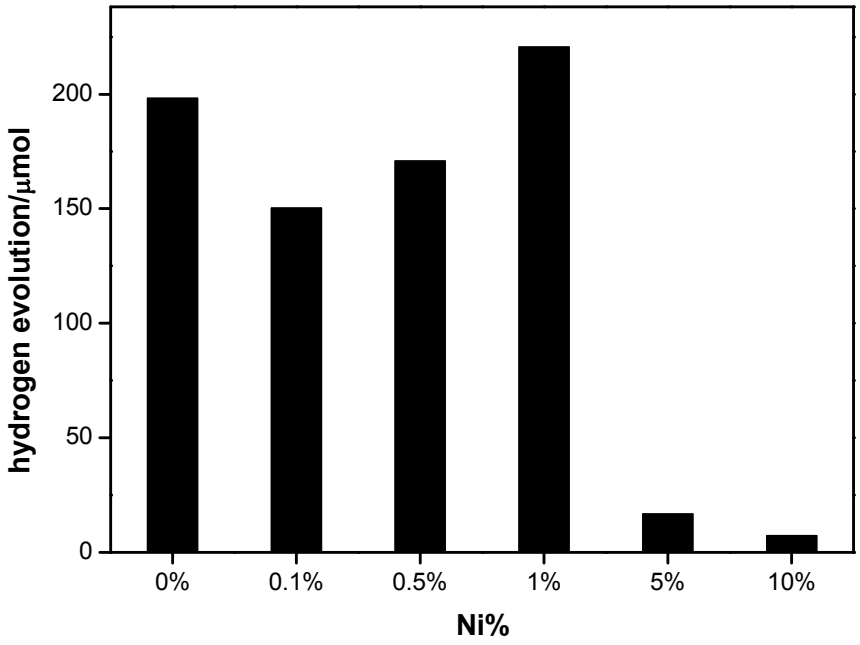

Figure 7: Hydrogen evolution of all the samples under 350W Xe lamp irradiation.

Acknowledgements

This research was financially supported by the National Basic Research Program of China (Grant 2009CB220000).

References

[1] Hu X.L., Li G.S., and Yu J.C., Design, Fabrication, and Modification of Nanostructured Semiconductor Materials for Environmental and Energy Applications. Langmuir, 2010. 26(5): p. 3031-3039.

[2] Serrano E., Rus G., and Garcia-Martinez J., Nanotechnology for sustainable energy. Renewable & Sustainable Energy Reviews, 2009. 13(9): p. 2373-2384.

[3] Mor G.K., et al., A review on highly ordered, vertically oriented tio2 nanotube arrays: Fabrication, material properties, and solar energy applications. Solar Energy Materials and Solar Cells, 2006. 90(14): p. 2011-2075.

[4] Hashimoto K., Irie H., and Fujishima A., TiO2 photocatalysis: A historical overview and future prospects. Japanese Journal of Applied Physics Part 1-Regular Papers Brief Communications & Review Papers, 2005. 44(12): p. 8269-8285.

[5] Guo L.J., et al., Solar hydrogen production and its development in China. Energy, 2009. 34(9): p. 1073-1090.

[6] Yu J.C., et al., Effects of F- doping on the photocatalytic activity and microstructures of nanocrystalline tio2 powders. Chemistry of Materials, 2002. 14(9): p. 3808-3816.

[7] Choi W.Y., Termin A., and Hoffmann M.R., the Role of Metal-ion Dopants in Quantum-sized TiO2 - Correlation between Photoreactivity and Charge-carrier Recombination Dynamics. Journal of Physical Chemistry, 1994. 98(51): p. 13669-13679.

[8] Wan B., et al., Preparation of Ag/TiO2 Nanotube and Its Photocatalytic Performance. Rare Metal Materials and Engineering, 2009. 38(11): p. 2012-2016.

[9] An H.Q., et al., Deposition of Pt on the stable nanotubular TiO2 and its photocatalytic performance. Catalysis Communications, 2009. 11(3): p. 175-179.

[10] Li Y.X., et al., Formation of multilayer-Eosin Y-sensitized TiO2 via Fe3+ coupling for efficient visible-light photocatalytic hydrogen evolution. International Journal of Hydrogen Energy, 2009. 34(14): p. 5629-5636.

[11] Jin Z.L., et al., 5.1% Apparent quantum efficiency for stable hydrogen generation over eosin-sensitized CuO/ TiO2 photocatalyst under visible light irradiation. Catalysis Communications, 2007. 8(8): p. 1267-1273.

[12] Chatterjee D., Effect of excited state redox properties of dye sensitizers on hydrogen production through photo-splitting of water over TiO2 photocatalyst. Catalysis Communications, 2010. 11(5): p. 336-339.

[13] Liu Y.L., et al., A composite visible-light photocatalyst for hydrogen production. Journal of Power Sources, 2006. 159(2): p. 1300-1304.

[14] Yang H.H., et al., A novel composite photocatalyst for water splitting hydrogen production. Journal of Power Sources, 2006. 159(2): p. 1305-1309.

[15] Jing D.W., Zhang Y.J., and Guo L.J., Study on the synthesis of Ni doped mesoporous TiO2 and its photocatalytic activity for hydrogen evolution in aqueous methanol solution. Chemical Physics Letters, 2005. 415(1-3): p. 74-78.

[16] Zhang W.F., Zhang M.S., and Yin Z., Microstructures and visible photoluminescence of TiO2 nanocrystals. Physica Status Solidi a-Applications and Materials Science, 2000. 179(2): p. 319-327.

[17] Wang Y.W., et al., Polyol-Mediated Synthesis of Ultrafine TiO2 Nanocrystals and Tailored Physiochemical Properties by Ni Doping. Journal of Physical Chemistry C, 2009. 113(21): p. 9210-9217.

[18] Ma L.J. and Guo L.J., Study on the thermo-Raman spectrum of TiO2 prepared with different precursors. Acta Chimica Sinica, 2006. 64(9): p. 863-867.

[19] Takeuchi M., et al., Investigations of the structure of H2O clusters adsorbed on TiO2 surfaces by near-infrared absorption spectroscopy. Journal of Physical Chemistry B, 2005. 109(15): p. 7387-7391.

[20] Kormann C., Bahnemann D.W., and Hoffmann M.R., Preparation and Characterization of Quantum-size Titanium-dioxide. Journal of Physical Chemistry, 1988. 92(18): p. 5196-5201.

[21] Yu J.G., et al., The effect of calcination temperature on the surface microstructure and photocatalytic activity of TiO2 thin films prepared by liquid phase deposition. Journal of Physical Chemistry B, 2003. 107(50): p. 13871-13879.

[22] Jianying S., et al., Photoluminescence characteristics of TiO2 and their relationship to the photoassisted reaction of water/methanol mixture. Journal of Physical Chemistry C, 2007. 111(2): p. 693-699.